



Realization of polymer charge pump circuits using polymer semiconductors

Senol Mutlu*, Iskender Haydaroglu, Ali Osman Sevim

Department of Electrical and Electronics Engineering, Bogazici University, 34342 Istanbul, Turkey

ARTICLE INFO

Article history:

Received 28 July 2010

Received in revised form 22 October 2010

Accepted 14 November 2010

Available online 2 December 2010

Keywords:

Charge pump circuit

AC–DC converter

Polymer diode

Poly(3-hexylthiophene)(P3HT)

ABSTRACT

Vertical diodes made of chromium/gold/poly(3-hexylthiophene) (P3HT)/aluminum are used to implement AC–DC charge pump circuits. A single stage polymer charge pump with 470 nF capacitors is able to supply 7.2 V DC to a load of $1\text{ M}\Omega \parallel 20\text{ pF}$ when an AC signal with a peak value of 10 V is applied. The circuit can be used up to 10 kHz. High turn-on voltages and internal resistances and capacitances of the diodes limit the DC output voltages. The ramp-up time of the circuit built with 10 nF capacitors is 9.4 ms for a 1 kHz, 10 V peak AC signal. Diodes are modeled and simulated in SPICE using space charge limited conduction model. The simulated charge pump circuit produces consistent results with measurements. Performances of air exposed vertical diodes deteriorate under vacuum, prolonged operation at atmospheric conditions and electrical bias stress resulting in blistering, emphasizing the importance of packaging the devices under inert atmosphere. The DC output voltage and the input impedance of the circuit can be adjusted by using multiple stages.

© 2010 Elsevier B.V. All rights reserved.

1. Introduction

Current electronic circuits made of polymer semiconductors may require very high supply voltages in the range of tens of volts [1]. Similarly, micromachined capacitive actuators require voltages in the same high levels [2]. Without a scheme to step up the supply voltages available from a commercial battery, portable applications of polymer semiconductor devices would be impractical. Furthermore, the potential for low cost and high volume fabrication makes polymer semiconductors attractive in a particular area, the polymer RFID tag. In this application, the power necessary for device operation needs to be transmitted wirelessly, in order not to include a battery that would drastically increase the cost of the device. Several approaches for the extraction of DC power from an RF signal are present, and a previous work shows a possible solution with two half-wave rectifiers to constitute the ground and supply rails of the RFID circuitry using diodes made out of pentacene [3]. This design confines the tag

supply voltage to the peak-to-peak voltage of the RF signal picked up by the tag antenna, minus twice the turn-on voltage of the diodes, which tend to be high in current polymer electronics. The charge pump method has been evaluated favorably to the half-wave rectifier scheme in RFID applications [4], for the charge pump approach gives more flexibility to designer in many ways. Cascading multiple stages of charge pumps allows the designer to adjust the supply voltage levels as desired and compensate for the large voltage drops across diodes. In addition, the input impedance of a charge pump depends on the number of stages and the loading of the charge pump [5], which allows the designer to perform impedance matching to the antenna that feeds the charge pump, maximizing the extracted power [4]. This leads to the reasoning that charge pump circuits built with polymer semiconductors are worthwhile to explore.

Polymer and organic diode half-wave rectifiers were built in previous literature using P3HT [6,7], as well as other organic/polymer semiconductor materials such as PTAA [8], pentacene [3,9–11], and hybrid p–n junction organic diodes using n-ZnO/(PQT-12) [12], and their AC characteristics were demonstrated. For high performance

* Corresponding author. Tel.: +90 2123597442; fax: +90 2122872465.

E-mail address: senol.mutlu@boun.edu.tr (S. Mutlu).

organic semiconductors such as pentacene, 3-dB cut-off frequencies of 15 MHz [9] to 50 MHz [10] were reported for half-wave rectifier topologies, the latter publication demonstrating that organic diodes can be operated at the 13.56 MHz RFID frequency with acceptable performance levels [10]. Half-wave rectifiers fabricated using P3HT, which can be solution-processed at relatively low cost, exhibit lower AC performance on the other hand. Cut-off frequencies between 1–1.8 MHz [7] and 2 MHz [6] were reported for half-wave rectifiers fabricated using this material.

In this work, a charge pump circuit built using regioregular poly(3-hexylthiophene) (rr-P3HT) is investigated, the aim being to meet the demand for high supply voltages in electronic devices fabricated from polymer semiconductors, as well as the possible application of wireless power transmission to polymer electronic devices. The charge pump topology that is featured in this work is shown in Fig. 1. This is a more useful method in generating supply voltages from RF signals, since the design is scalable as opposed to supplying power from a single half-wave rectifier. The number of charge pump stages determines both the DC levels of the output voltage and the input impedance of the charge pump itself.

In the design of the charge pump circuits, an electrical model for fabricated vertical diodes has been used. After the diodes are fabricated, their electrical model parameters are extracted and used in a computer aided design tool, simulation program with integrated circuit emphasis (HSPICE), to investigate the operation of the charge pump circuit. In the models, the environmental effects on the characteristics of polymer diodes are also studied. Since in polymer semiconductor the performances of devices are deteriorated by environmental variables such as oxygen, humidity, ambient temperature [13–15] and electrical bias stress, the parameters of the model are also changed accordingly. Parameter fittings for the model have been done to the vertical diodes using the results of experiments that expose them to the mentioned environmental variables.

This paper is organized in five sections. Section 2 describes the fabrication of lateral and vertical polymer diodes and presents their current–voltage characteristics

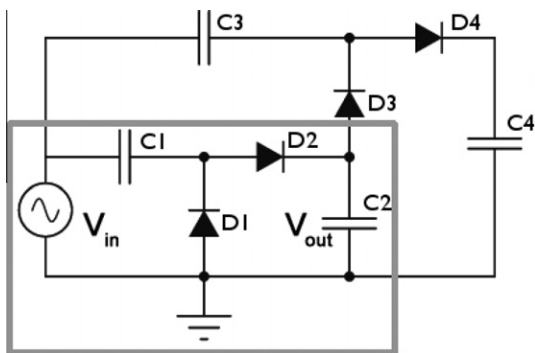


Fig. 1. Schematic representation of a multi-stage AC–DC charge pump. The gray box represents a single cell of a charge pump, the basic building block of a multi-stage design.

under various environmental conditions. Section 3 presents the theory and a model for the fabricated vertical diodes to be used in the charge pump circuits. Section 4 explains the operation of the charge pump circuit and gives experimental results for various conditions and compares them to the simulation results. Discussions and conclusion are given in Sections 5 and 6, respectively.

2. Polymer diodes

Polymer diodes are the main components of this work. They are fabricated, characterized and modeled before they are used in a charge pump circuit. Since polymer diodes are not stable under ambient conditions and they degrade, they are also tested for their changing performances under ambient conditions to check whether degradations can be modeled and predicted or tolerated in certain circuit applications. For this purpose, two types of diodes have been fabricated and tested; lateral and vertical diodes. The main purpose of the fabrication of the lateral diodes were to study the environmental effects on semiconductor polymers more easily since its active polymer is directly in contact with the environment. Its surface is not covered with a metal film.

2.1. Lateral diodes

2.1.1. Fabrication of lateral diodes

In fabricating lateral diodes, two electrodes of the diodes are fabricated in plane in an interdigitated manner. The aluminum cathode and the silver-epoxy anode are deposited on top of the glass substrate such that the diode, from the top view, resembles a system of interlocking fingers as drawn in Fig. 2. 90 nm thick aluminum is thermally evaporated on a glass substrate and patterned using lithography. Silver electrodes are formed by drop-casting a silver epoxy liquid and then cured on a hotplate at 110 °C. A sharp metal tip with a reservoir filled with silver epoxy is attached to a micromanipulator and is moved to make the silver electrodes between aluminum ones. This limited the gap size between electrodes to 300 μm. The total length of the diode formed by the interdigitated layout is measured to be 10.5 mm and the gap between the electrodes 300 μm. After the deposition of the electrodes, rr-P3HT (from Sigma–Aldrich) solution is deposited by drop-casting and annealed for one hour at 110 °C to evap-

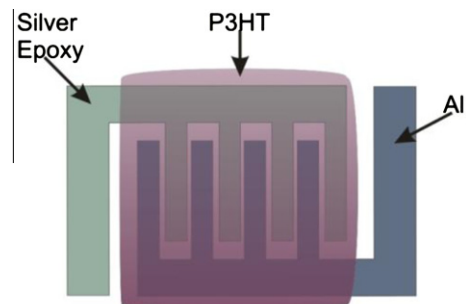


Fig. 2. Top view of the interdigitated lateral diode.

orate solvent. The polymer is dissolved in 1,2,4-trichlorobenzene with a weight concentration of 2.5 mg/ml and filtered through a 0.2 μm pore sized PTFE membrane syringe filter.

2.1.2. Experimental results of lateral diodes

Following fabrication, the lateral diodes stayed at ambient conditions for a day. Then, they are placed into a vacuum chamber and 30 mTorr vacuum is achieved inside the chamber before the characterization of the devices are initiated. DC voltage sweeps are conducted with Keithley semiconductor parameter analyzer (SCS4200) and the current through the diodes are measured at varying time intervals after the start of the vacuuming to investigate the effects of time under sustained vacuum on device performance. Results are summarized in Fig. 3. Vacuum treatment of the lateral diodes resulted in the decrease of both forward and reverse currents, indicating a drop in the parasitic conductivity. This is expected since the vacuum dedopes the semiconductor polymer by removing the atmospheric oxygen inside, which has been absorbed during the fabrication steps done at room conditions. Atmospheric oxygen is known to dope semiconductor polymer, thus create parasitic conductivity [1]. As the vacuum is maintained, reverse current diminishes more rapidly than the forward current, increasing the rectification ratio of the diode. The ratio of the diode's currents at a forward bias of 7 V and a reverse bias of 7 V is around 2 just before the vacuum started. This ratio increases to 240 after 4 h of vacuuming.

After vacuum tests, the chamber pressure is brought to 1 atm by releasing argon gas into the chamber. Being a noble gas, argon is used to eliminate the possibility of P3HT to react with doping agents such as oxygen and water vapor that would have been present had the experiment been conducted at atmospheric conditions. After the desired pressure is obtained, the diodes are heated to varying temperatures and current–voltage measurements are acquired after 5 min of maintaining the desired temperature. This waiting period is needed for the front surface of the glass wafer, where the diodes are, to reach the desired temperature. The results are shown in Fig. 4. Elevated temperatures resulted in a dramatic increase in forward current as well as the rectification ratio in lateral diodes. As theory suggests, the P3HT thin film, when formed, is an amorphous

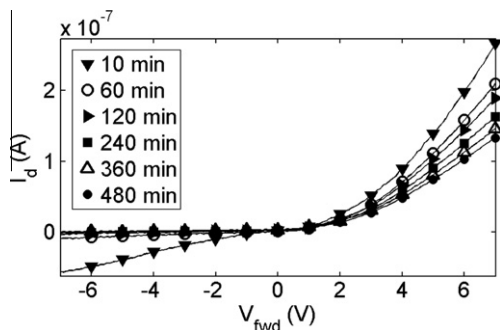


Fig. 3. Change in current–voltage characteristics for lateral diode under vacuum with elapsing time.

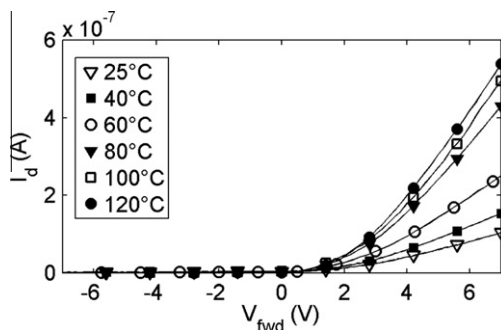


Fig. 4. Lateral diode current–voltage characteristics recorded at various temperatures.

composition of grains of polymer. The charges cannot hop between two neighboring grains unless the energy barrier constituted by the intergrain boundary, called a trap state, is overcome [15,16]. Elevated temperatures causes the excitation of a greater number of these trap states, which enables charges to move across the trap states. The end result is an increase in current density for a given voltage, increasing the performance of the diode. The improvement is not sustained after the temperature is reduced back to room temperature [17]. Therefore, it is determined that annealing of the thin film P3HT does not occur in lateral diodes in the applied temperature range of this work [18]. As a result of heating from 25 $^{\circ}\text{C}$ to 120 $^{\circ}\text{C}$, the forward current increases from around 100 nA to 540 nA at 7 V forward bias. Similarly, rectification ratio of around 80 at 25 $^{\circ}\text{C}$ increases to 900 at 120 $^{\circ}\text{C}$.

As observed in the vacuum tests, the rectification ratio of the lateral diode is improved by vacuum treatment, which can be preserved by an adequate packaging of the device following the vacuum treatment. The rectification ratio, which can also be referred to as the on–off ratio, is of vital importance in a charge pump application since a diode that leaks current when it is supposed to behave like an open circuit detracts from the efficiency of the charge pump. Despite the potential performance improvement, the lateral diode can provide small amounts of forward current (around 100 nA) since in this work electrode space is large, around 300 μm , forming a high parasitic resistance in series with the diode. This makes it ineligible for a charge pump application in which the charge pump acts as a current source for resistive current loads in need of about 10 μA . However, this electrode gap can be easily made to around 1 μm if another metal thin film such as Chromium (Cr)/Gold (Au) is evaporated and lithographically patterned. In that case it could conduct more current for the same voltage applied. Nevertheless, vertical diodes whose electrode gap between anode and cathode is the thickness of the polymer, would have less resistive parasitic and can supply more current than lateral diodes. However, one advantage of lateral diode may be that its semiconductor polymer is exposed to the environment directly. Since the semiconducting polymer is not capped with another thin film metal, it can be treated thermally or with vacuum much easier than the packaged one.

2.2. Vertical diodes

2.2.1. Fabrication of vertical diodes

The fabrication of the vertical diodes involves sandwiching the drop casted P3HT layer between two metal layers. While the bottom electrode is deposited by a high vacuum evaporator and patterned by lithography, the top electrode is formed by means of shadow mask evaporation. Alignment errors and the spread of the deposited metal in shadow masking cause deviations from designed device sizing.

The process sequence of the fabrication, as shown in Fig. 5, starts by lithographically patterning the thermally evaporated Cr/Au thin films to form bottom electrodes. Similar to the lateral diode fabrication, P3HT is dissolved in trichlorobenzene with a ratio of 2.5 mg/ml. This solution is drop-casted and is left to dry on the substrate at room conditions for 2 h, resulting in a film thickness of approximately 750 nm. For the deposition of the aluminum electrodes, a shadow mask is prepared from a 50 μm thick stainless steel (SS301) sheet. A photoresist mask is patterned on steel surface using lithography and then steel is isotropically etched using electrochemical etching in 1:7 HCl:DI water solution [19]. A vacuum chamber with a base pressure of 10^{-6} Torr is used to evaporate a 90 nm thick aluminum layer. The shadow mask is aligned perpendicular to the patterned Cr/Au electrodes and evaporation forms orthogonal aluminum electrodes resulting in diodes with active area of 2 mm \times 0.5 mm.

2.2.2. Experimental results of vertical diodes

Similar to the lateral diode tests, vertical diodes are subjected to vacuum and elevated temperatures to determine the effects of atmospheric doping and thermal activation on them. Additionally, a set of diodes are operated under atmospheric exposure to observe the degradation of performance that is expected to happen as the P3HT thin film deteriorates.

Diodes tested under atmospheric conditions are kept at these conditions for a week before they are electrically tested. During tests, they continued to get exposed to atmospheric conditions. The results are presented in

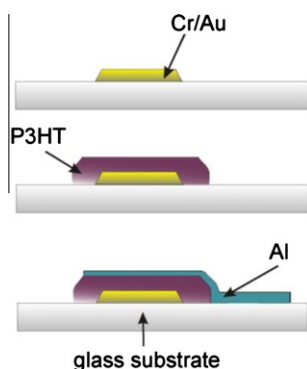


Fig. 5. Fabrication steps for polymer charge pump circuits, from top to bottom: evaporation of Cr/Au contacts, deposition of P3HT, followed by the evaporation of aluminum through a shadow mask.

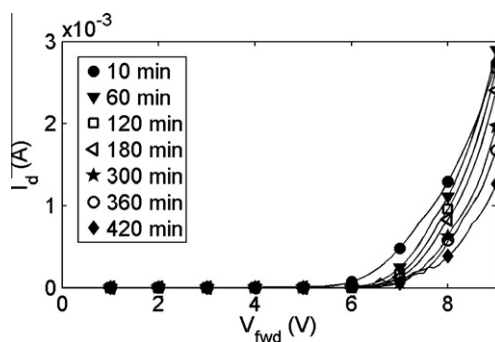


Fig. 6. Current-voltage characteristics of the vertical diode under atmospheric exposure with elapsing time.

Fig. 6. The diodes continue to operate without much degradation in forward current up to 60 min after the start of the tests. Forward current is recorded to be around 1.2 mA at 8 V forward bias during this interval of time. The decline in forward current is discernible at 180 min, and after 420 min the forward current suffers drastically. This part of the experiment reveals that operation under atmospheric exposure causes the deterioration of device performance.

Deterioration of the behavior of the diodes is correlated to changes in their physical appearance. The vertical diodes exhibited blistering under the top aluminum cathode of the diode as shown in Fig. 7. The existing bubbles and blisters are inflated with device operation, and new blisters emerge as tests are performed. Similar blistering was reported in P3HT-PEDOT systems [13] and in inkjet printed P3HT devices [14]. The explanation for this phenomenon was identified as the electrolysis of the atmospheric impurities such as water vapor that has dissolved inside the P3HT thin film with electrical bias stress. The resulting gases would try and escape the thin-film, but they would encounter the top electrode, where they form the observed blisters. Blistering mechanism might be a contributing factor in the decrease in diode forward current with time; since the bubbles break the integrity of the P3HT-Al interface where they form, thereby reducing device efficiency.

Vacuum treatment of the vertical diodes with the conditions mentioned at the lateral diode section reveals worse degradation than the atmospheric results. Current-voltage characteristics of the vertical diode just after vacuuming started are shown in Fig. 8. Diodes have been at atmospheric conditions for a day after their successful fab-

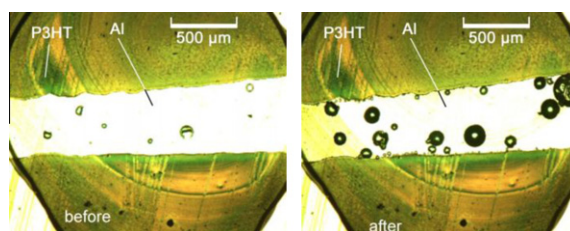


Fig. 7. Before (left) and after (right), operation of vertical diodes under atmospheric conditions.

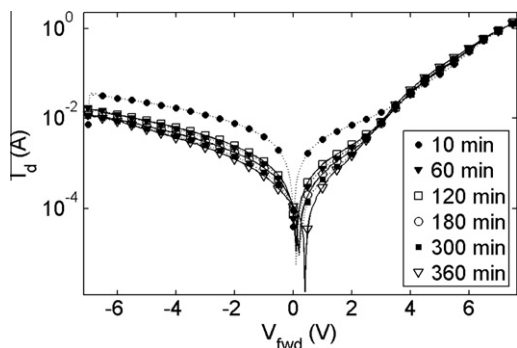


Fig. 8. Semilog plots for the current–voltage characteristics showing the effects of vacuum treatment on vertical diodes with elapsing time.

rication. At the beginning of the tests certain improvement in diode performance occur since the vacuum starts to extract the dopants inside the polymer, thus decreases the leakage currents in the reverse bias. However, the measured current–voltage curves deteriorate after some time. These deviations could be the result of an increasing number of blisters as the device is subjected to electrical bias stress. Severe deterioration on the aluminum surface due to vacuum and operation can be seen in Fig. 9. The blistering observed under vacuum treatment is extensive, resulting in comparatively smaller but far more numerous blisters beneath the top electrode, in contrast with devices tested under atmospheric conditions. A possible explanation for this is that the applied vacuum sucks out the dissolved impurities from the thin-film, collecting a portion of them under the top electrode through which they cannot diffuse away. The applied bias stress causes the electrolysis of these impurities, resulting in the blisters. Since vacuum drives a larger amount of impurities in comparison to the air exposed diodes, the blisters are numerous and cover the layer beneath the top electrode almost entirely. This also explains why these deteriorations are not observed on lateral diodes. Since the top of the lateral diode is not blocked by a thin metal film, vacuum treatment improves the diode performance with time steadily.

This situation for the vertical diodes may be avoided if a slower and gradual increase of vacuum is applied with thermal annealing to give a chance to dissolved impurities to leave the device surface without causing any deformation. Starting vacuum treatment at a lower vacuum value such as 150 Torr and then gradually and slowly increasing the vacuum while keeping the samples at elevated temper-

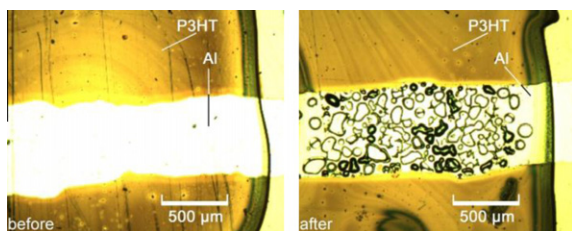


Fig. 9. Before (left) and after (right) operation of vertical diodes under vacuum.

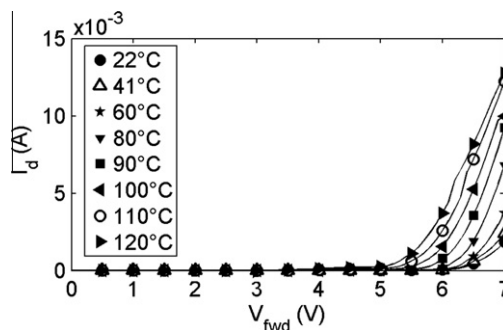


Fig. 10. Current–voltage characteristic of vertical diode at elevated temperatures.

atures such as 90–110 °C may avoid blisters on the surface. During this time, the devices should not be operated. After this postfabrication treatment, the devices can be packaged under these conditions [20].

A separate vertical diode is subjected to elevated temperatures under argon gas environment with the pressure maintained at around 1 atm. Before this test, the diode stayed at atmospheric conditions for a week. Similar to the performance improvement of lateral diodes at elevated temperatures, the vertical diodes are also observed to conduct more current at the same voltage values as the temperature is increased, as shown in Fig. 10. The thermal activation of the intergrain boundaries results in more carriers with enough energy to cross the trap states. As a result of heating, the forward current increases from around 2 mA to 12 mA at 7 V forward bias as the temperature increased from 22 °C to 120 °C. Lowering the temperature back to the initial temperature values does not sustain the improvement, leading to the conclusion that annealing of the thin-film did not occur in the process.

3. Polymer diode model

Simulation models for organic and polymer diodes have been reported, modeling the properties of various organic and polymer semiconductors with a voltage dependent mobility factor [21,22]. A more straightforward approach in modeling both organic [9] and organic–inorganic hybrid [12] diodes features two diodes connected in parallel but in reverse directions, one diode modeling the forward current component while the other modeling reverse current component. Both approaches produce good results in modeling the DC behavior of the measured characteristics; however it is found that the approach that makes use of voltage varying mobility produces a more accurate model of the charge pump operating at higher frequency ranges and for different values of peak amplitudes of input voltage.

Under high electric fields, (reported to be in the order of 10^5 V/cm for P3HT [22]) space charge limited conduction (SCLC) is dominant in polymer semiconductors such as P3HT [22]. In SCLC regime, current conduction is dominated by Mott–Gurney equation:

$$J = \frac{9}{8} \cdot \frac{\epsilon_0 \epsilon_r}{d^3} \cdot \mu \cdot V^2 \quad (1)$$

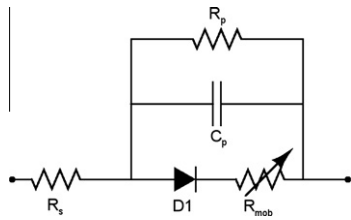


Fig. 11. Circuit model for the P3HT vertical diode.

where μ is the voltage dependent mobility, ϵ_0 is the electrical permittivity of air, ϵ_r is the dielectric constant of the polymer. V represents the voltage across the diode and d the thickness of the polymer film, estimated to be around 750 nm for this work. The voltage dependent mobility is expressed as follows:

$$\mu = \mu_0 \cdot e^{0.89 \cdot \gamma \sqrt{V/d}} \quad (2)$$

where μ_0 is the zero-field mobility and γ is the electric field prefactor [22]. Including the voltage dependent mobility within the Mott–Gurney equation integrates the Frenkel effect into the model, emulating the effects of trap states within the polymer film. This yields a more accurate model since the rapid departures from the original Mott–Gurney equations, resulting from high electric field ranges, are now taken into account [23]. In low field regimes, current voltage characteristics of our device model, shown in Fig. 11, are dominated by the diode element, modeling the effects of Schottky contact. As the device enters SCLC regime, the current through the device is dominated by the modified Mott–Gurney equation that includes the Frenkel effect. This latter current regime is modeled by the voltage varying resistor R_{mob} in an approach similar to the work in [21].

The procedure for fitting the model to the measured data starts with fitting the model to the DC sweep measurements of the diode, which gives the reverse saturation current, I_S , and the ideality factor, N , in the SPICE model of the diode element and series and parallel resistances, as well as field-dependent mobility parameters. Junction capacitance, C_{JO} , in the SPICE model of the diode element is due to the depletion region caused by the Schottky contact between P3HT and aluminum. Junction capacitance value is estimated to be in the proximity of 100 pF based on the area of the diode and data reported in previous work on rr-P3HT/aluminum Schottky contact, which estimates the depletion width to about 170 nm for zero voltage bias [24]. The parasitic capacitance, C_p , is simply a parallel plate capacitor formed by the two metal electrodes and the polymer film in-between. It is set to 36 pF, based on the approximated polymer thickness of 750 nm, the relative permittivity of 3.0 [13], and an active device area of 1 mm². Transit time parameter, TT , in SPICE diode model, was also set to 150 μ s to fit the model to the measurements. The model was simulated in HSPICE.

4. Charge pump circuits

Charge pump circuit is built using two of the fabricated vertical polymer diodes and two external capacitors. Its

operation principle and the experimental results are given in the sections below.

4.1. Operation of the charge pump circuit

Assuming an alternating signal is applied as the input voltage to the charge pump circuit shown in Fig. 1, the negative cycle of the input switches diode D1 on while D2 remains turned off, allowing the capacitance C1 to charge up to the peak voltage of the applied signal. In this situation, D1 and C1 work as a clamper. The following positive cycle of the signal reverse biases D1 and forward biases D2. As a result, C2 is charged up to a positive peak voltage that is the sum of the peak voltage of the applied signal and the voltage stored in C1 from the previous cycle. In this situation, D2 and C2 form a half-wave rectifier. The two terminals of C2 can be used as a DC voltage source, yielding a DC level with some small ripple voltage superposed that is twice the peak voltage of the applied signal under ideal circumstances such as very small stray capacitances along with negligible diode turn on voltages. If a second stage is appended to the first stage, D3 would have its cathode connected to the DC output voltage of the prior stage, and the output voltage that is observed over C4 would be four times that of the peak amplitude of the applied signal.

A typical charge pump circuit given in Fig. 1 can have K stages. Each stage can have identical diodes with turn-on voltage of V_{on} and identical capacitors with capacitance of C . The output of this circuit, V_{out} , can be made to supply a current of I_{out} at the output when an AC signal with a frequency of f and a peak voltage of V_{peak} is applied to the input. Since there would also be stray capacitances, C_s , at the nodes that diodes are connected, a simple output equation for this charge pump circuit can be expressed as [5]:

$$V_{out} = 2 \cdot K \cdot \left[\frac{C}{C + C_s} \cdot V_{peak} - V_{on} - \frac{I_{out}}{(C + C_s) \cdot f} \right] \quad (3)$$

It can be observed from this equation that the stray capacitances diminish the peak voltage on the output by sharing the stored charge within the charge pump capacitors, C . Eq. (3) fails to include the diminishing effects of the parasitic parallel plate capacitance, C_p , and the junction capacitance, C_{JO} , of the diodes on the peak voltage. These parasitic capacitors must also be lumped to C_s to get a more accurate analytical result. Numerical results acquired from the simulations of HSPICE take the effects of these capacitors into account.

As a minimal requirement, the single stage polymer charge pump is designed to deliver 10 V DC when an oscilloscope probe is connected to its output node. The oscilloscope probe presents a 1 M Ω || 20 pF load to the charge pump. This load is similar to a load that is formed by multiple polymer transistors that we fabricate. Our typical polymer transistor passes a drain current of around 1 μ A when a source-drain voltage of -40 V is applied to turn it on. The continuous, resistive current load provided by the oscilloscope brings down the DC output levels according to Eq. (3). The continuous resistive loading is a realistic model for a charge pump circuit driving multiple polymer transis-

tors, where current leakage is significant even if the devices are turned off.

4.2. Experimental results of charge pump circuits

Fabricated charge pumps are tested with external capacitors of 470 nF added on, soon after the completion of the fabrication of vertical diodes. Tests are conducted under argon environment after diodes have been exposed to atmosphere for about a week. These results are shown in Fig. 12. The frequency response of a single stage charge pump for different peak voltages of the input AC signal reveals that the device operates at reasonable output levels up to 1 kHz and it could possibly operate acceptably at around 10 kHz.

Simulation results for the charge pump circuit using the models developed for the vertical polymer diodes are also plotted in Fig. 12. In order to do this, first, the DC current–voltage characteristics of the vertical diodes are measured. Then, the DC parameters for the model described in Section 3 are extracted from these DC measurements. The measured DC current–voltage characteristics and the simulation results done with the extracted parameters are shown in Fig. 13. This figure shows a good match between them. Using these DC parameters, the AC characteristics of the model are also fit to the measurements, shown in Fig. 12.

The experimental and simulation results of the charge pump circuit in Fig. 12 are mostly in agreement. The observable mismatch between the experimental measurements and the simulation results, visible in the 7 V, 6 V and 5 V curves in Fig. 12, can be explained by the fact that the diodes are not under high enough electric fields at these voltage values to meet the SCLC condition that is assumed in this model [22]. For a peak voltage of 7.5 V and an estimated polymer thickness of 750 nm, the electric field becomes 10^5 V/cm, residing in the reported regime where SCLC becomes dominant for P3HT [22]. Above this voltage, i.e. for 8 V, 9 V and 10 V curves in Fig. 12, the featured SCLC model is highly accurate.

Following these tests, charge pump circuits using various capacitor sizes are built and tested. For different charge

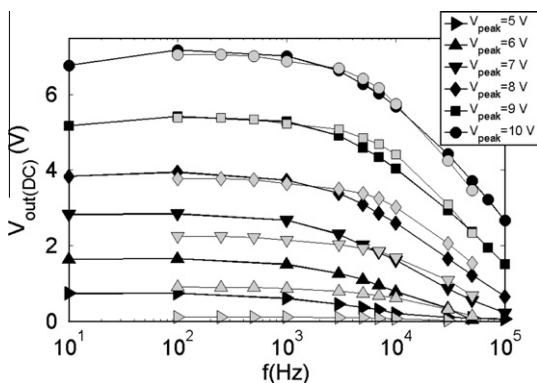


Fig. 12. V_{out} vs. frequency plots for various V_{peak} values of the AC input, $C_{pump} = 470$ nF. Simulation results are in grey and measurement data in black.

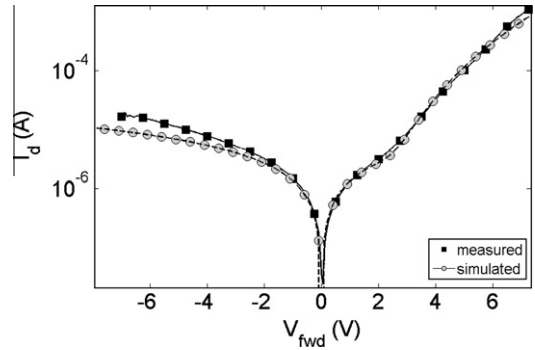


Fig. 13. Simulated and measured DC current–voltage characteristic of the fabricated vertical diodes.

pump capacitors, output voltages are measured as the frequency of the applied AC signal with a peak voltage of 10 V is changed. The results are summarized in Fig. 14. A drastic reduction in output voltage is observed as the pump capacitors are lowered from 68 nF to 10 nF, implying that the stray capacitance is relatively close to, but smaller than 10 nF, since the circuit can still operate with 10 nF capacitors. Simulation results using the diode model are also plotted on this figure.

It is observed that the model parameters fitted for diodes of the charge pump circuit with a fixed capacitor of 470 nF given in Fig. 12 do not fit accurately to the results of the output voltage measurements done using lower pump capacitors such as 68 nF and 10 nF shown in Fig. 14. Variances between the model parameters that are used to fit the former and latter measurements, the 470 nF and 10–68 nF cases, respectively, are reported in Table 1. CJO , N and IS are SPICE parameters defining the diode, and parameters B and u_0 belong to voltage dependent mobility element, electric field prefactor and zero-field mobility, respectively. This inaccuracy can be attributed to the degradation of the aluminum–P3HT interface with prolonged usage. The blisters that are induced due to electrical bias stress cause imperfections within the metal–semiconductor interface, where Schottky contact occurs. Since the initial measurements are made using

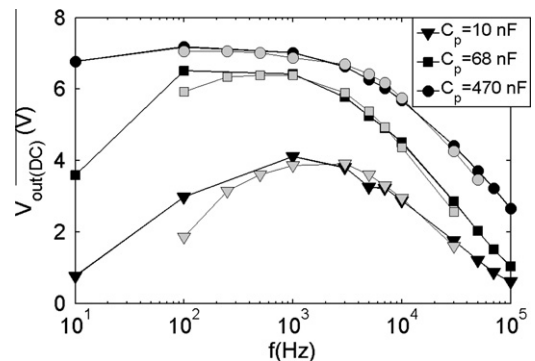


Fig. 14. V_{out} vs. frequency plots for various pump capacitors using AC signals with peak voltages of 10 V. Simulation results are in grey and measurement data in black.

Table 1

Varying model parameters used to fit two separate measurement runs; 470 nF and 68–10 nF cases.

Parameters	470 nF	10 nF & 68 nF
CJO	0.1n	0.5n
N	10.5	11.5
IS	$2.5e-14$	$25e-14$
B	$1.25e-2$	$1.8e-2$
u_0	$1.75e-6$	$0.2e-6$

470 nF capacitors, the model parameters that are required to fit the simulation results to the measurements are closer to the ideal than the latter charge pumps tested with 68 nF and 10 nF capacitors, using degraded diodes from previous use.

The expected effects from the increased number of defects due to the deterioration of the aluminum-P3HT interface include charge trapping within the defects and increased dependence of mobility on electric field. Charge trapping effects observed in similar vertical structures of aluminum-P3HT diodes have been modeled as capacitors parallel to depletion capacitor in the literature [25]. Trapping action due to the increased number of defect sites is incorporated into the junction capacitance in our model as an approximation, the reason being that the defects are occurring at the aluminum-P3HT interface where depletion capacitance also forms, increasing the overall junction capacitance in the deteriorated diode samples.

In addition to the measurements showing how the output voltage of the charge pump circuit changes with the frequency and the peak voltage value of the AC input, ramp-up times of charge pump circuits with various capacitor sizes are investigated. The operation of the charge pump may require a rapid rise time to the final output voltage value. For example in an RFID scenario, the reception of the RF signal must result in the power-up of an RFID tag as soon as possible or data might be lost during the process. Measured ramp-up times are shown in Fig. 15 for an input AC signal with a peak voltage of 10 V at 1 kHz frequency. The final output voltage is reached within 9.4 ms in charge pumps that used 10 nF, 32.5 ms for 68 nF and 205 ms for 470 nF designs. The ramp-up time for 470 nF case is much greater than 68 nF and 10 nF cases,

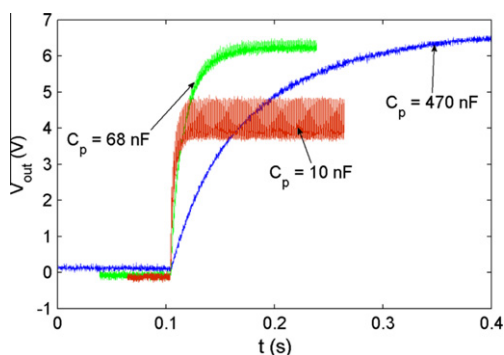


Fig. 15. Ramp-up waveforms for charge pumps built with various pump capacitors, with oscilloscope data for 470 nF, 68 nF and 10 nF cases superposed for comparison purposes. AC input signals are applied with a peak voltage of 10 V at frequency of 1 kHz.

and might be slow even for polymer electronics applications. The final DC levels reached in this figure are close to each other for the charge pump circuit with 470 and 68 nF capacitors, similar to the results in Fig. 14. However, charge pump circuit with 470 nF capacitors has smaller ripple voltages than the one with 68 nF.

5. Results and discussion

Experimental results from the lateral and vertical diodes reveal that the deterioration in their performance when operated under atmospheric conditions is drastic. This emphasizes the importance of packaging the devices under inert atmosphere, thus preserving the diodes in their best states. Considering that current-voltage characteristics that approximate an ideal switch is pivotal in the operation of the charge pump circuit, packaging process becomes as important as the design of the charge pump.

The thermal experiments reveal that both lateral and vertical diodes benefit from increased temperatures within a certain range. It is determined that the on/off ratios of the diodes improve invariably when the ambient temperature is raised from room temperature to 120 °C. This improvement in performance has been explained by the thermal activation of trap states formed by the boundaries between grains of polymer. Improvement in on-current is not sustained when the diodes are brought back to room temperature, therefore it is reasoned that thermal annealing does not take place within the temperature range that is used during the experiments.

The charge pump built using vertical polymer diodes in this work is considered to be the building block of larger charge pumps. The best case output voltage expected from the charge pump is, according to Eq. (3), twice the difference between AC input peak voltage and the turn-on voltage of the diodes. The output voltage can be improved by a peak voltage much larger than the turn-on voltage of the diode, which is roughly around 5 V in this work, and charge pump capacitors much greater than the stray capacitances, including the junction capacitances of the diodes. To ensure the best case condition in terms of capacitances, 470 nF capacitors are used, diminishing the effect of stray capacitances. For a peak voltage of 10 V, expecting an output load current of around 10 μ A, the best case output voltage would be 9.6 V from this single stage charge pump. In meeting the above conditions, we have observed output voltages of 7.2 V between 100 Hz and 1 kHz frequency range, 75% of the calculated best case output voltage of the single stage charge pump under these conditions. The probable source of error is the parasitic internal resistances and capacitances of the diodes formed as a result of deterioration, which is caused by impurities inside under electrical bias stress. This causes the diodes to further deviate from the desired ideal switch behavior.

Another consideration is that the vertical diode with dimensions of 2 mm \times 0.5 mm is able to adequately supply currents within milliampere range but only tens of microamperes is required by the following electronic circuit composed of polymer transistors. Excessive diode area does not help if the extra current is not used by the circuit

at the load. In fact an excessively wide device area introduces larger stray capacitances to the charge pump, shares the charge that would otherwise be stored entirely on the pump capacitors and reduces the high frequency performance of the design, as reported in the literature for P3HT rectifiers [7]. Therefore, a minimal diode area that satisfies the design objectives must be sought for, without neglecting some additional device area to safely meet any possible fabrication error.

Even though the output voltage of this circuit is lower than expected due to the high turn-on voltage of the diodes, internal diode resistances and capacitances that are the result of the deterioration of the exposed P3HT and high stray diode capacitances, cascading a number of stages of such cells would recover the loss in voltage in the expense of efficiency and frequency response. The cascading of multiple cells of charge pump is not preferable, but might be necessary for matching purposes [4]. The number of stages in a charge pump, as well as its loading and its operation frequency, controls its input impedance [4,5], and by adjusting the input impedance of the charge pump, impedance matching to the antenna that drives the charge pump can be achieved in an RFID application.

Simulation models based on SCLC theory are shown to be accurate under high electric field conditions, given that necessary adjustments to the model are made to adapt the models for the physical deterioration that can be observed after prolonged electrical bias stress. It is determined that by increasing the diode capacitance and the ideality factor of the diode, along with increasing the electrical prefactor (to make the diode current more dependent on the applied voltage) and decreasing the zero-field mobility, as expected when physical defects are introduced to the aluminum-P3HT interface, the degradation effects can be expressed within the SCLC model. DC current–voltage characteristics of P3HT diodes are modeled using a similar approach [22], and we demonstrate that the SCLC model featured in this work is also accurate and practical for the transient simulation of P3HT diodes at varying frequencies.

Along with their potential use in future polymer RFID tags, the charge pump is also attractive for other battery-powered, portable polymer electronics applications where very high voltages would be needed for device operation but supplying such amplitudes from conventional batteries would be impractical. In such devices, such as flexible polymer displays and micromachined capacitive actuators, polymer charge pumps could be implemented on plastic substrate without using additional, dedicated integrated charge pump chips or charge pumps built from discrete elements, which would cause the cost of such a system to rise noticeably. The frequency limitations of the multi-stage charge pump would become less of a problem in such systems since a steady DC voltage would be all that is needed, in contrast with the RFID data transmission problem.

6. Conclusion

Lateral and vertical polymer diodes have been fabricated using P3HT. Evaluations of the performances of the

diodes were done under elevated temperature and vacuum/atmospheric exposure. Performances of air exposed lateral diodes improved continuously under vacuum since there was no metal film covering the polymer film. However, air exposed vertical diodes under vacuum and prolonged operation at atmospheric conditions showed deteriorated performances. Blistering of the vertical diodes was observed with electrical bias stress; and although the blistering was observed to be extensive under vacuum and air exposure, the performance of the devices operated under argon did not seem to suffer too much. Performances of both the lateral and vertical diodes under argon environment improved steadily when the ambient temperature was raised from room temperature to 120 °C. This was due to the thermal activation of trap states formed by the boundaries between grains of polymer. Improvement was not sustained when the diodes were brought back to room temperature indicating that thermal annealing did not take place. It was determined that protecting the device from atmospheric elements was necessary to preserve their current–voltage characteristics.

Circuit models have been developed for the vertical diodes. Transient simulations of P3HT diodes using SCLC model were demonstrated. Fabricated charge pumps using vertical diodes and various capacitors revealed similar results as the models predicted. Charge pump circuits were able to generate DC voltages from AC voltages in the frequency range from 100 Hz to 10 kHz. Generated DC voltage level was lower than ideal because of the high turn-on voltages of the diodes and their internal parasitic resistances and capacitances.

The simulation model was implemented in HSPICE and was practical to use. However, some modifications might be required to cover the smaller voltage amplitudes. Degradation effects that were observed under prolonged use of polymer diodes were incorporated into the model by modifying certain model parameters, which produced results consistent with experimental measurements.

Acknowledgement

This work is supported by the Scientific and Technological Research Council of Turkey (TUBITAK) under project EEEAG 106E013 and State Planning Organization of Turkey, TAM Project (2007K120610).

References

- [1] D.M. Russell, T. Kugler, C.J. Newsome, S.P. Li, M. Ishida, T. Shimoda, Doping of organic semiconductors, *Synthetic Metals* 156 (2006) 769–772.
- [2] E.T. Carlen, K.H. Heng, S. Bakshi, A. Pareek, C.H. Mastrangelo, High-aspect ratio vertical comb-drive actuator with small self-aligned finger gaps, *Journal of Microelectromechanical Systems* 14 (5) (2005) 1144–1155.
- [3] K. Myny, S. Steudel, P. Vicca, J. Genoe, P. Heremans, An integrated double half-wave organic Schottky diode rectifier on foil operating at 13.56 MHz, *Applied Physics Letters* 93 (2008) 093305.
- [4] D. Dobkin, *The RF in RFID*, Newnes, Oxford, 2008.
- [5] F. Pan, T. Samaddar, *Charge Pump Circuit Design*, McGraw-Hill, New York, 2006.
- [6] C.M. Kang, S. Kim, Y. Hong, C. Lee, Frequency analysis on poly(3-hexylthiophene) rectifier using impedance spectroscopy, *Thin Solid Films* 518 (2009) 889–892.

- [7] S. Kim, H. Cho, Y. Hong, C. Lee, Effect of electrode area on high speed characteristics over 1 MHz of poly(3-hexylthiophene-2,5-diyl) diode with inkjet-printed Ag electrode, *Molecular Crystals and Liquid Crystals* 513 (2009) 256–261.
- [8] K. Lilja, T.G. Bäcklund, D. Lupo, T. Hassinen, T. Joutsenoja, Gravure printed organic rectifying diodes operating at high frequencies, *Organic Electronics* 10 (2009) 1011–1014.
- [9] B.N. Pal, J. Sun, B.J. Jung, E. Choi, A.G. Andreou, H.E. Katz, Pentacene-zinc oxide vertical diode with compatible grains and 15-MHz rectification, *Advanced Materials* 20 (2008) 1023–1028.
- [10] S. Steudel, K. Myny, V. Arkhipov, C. Deibel, S. De Vusser, J. Genoe, P. Heremans, 50 MHz rectifier based on an organic diode, *Nature Materials* 4 (2005) 597–600.
- [11] S. Steudel, K. Myny, P. Vicca, D. Cheyns, J. Genoe, P. Heremans, Ultra-high frequency rectification using organic diodes, *Technical Digest International Electron Device Meeting – IEDS 2008*, pp. 93–96.
- [12] J. Sun, B.N. Pal, B.J. Jung, H.E. Katz, Solution-processed hybrid p–n junction vertical diode, *Organic Electronics* 10 (1) (2009) 1–7.
- [13] K. Rashmi, A. Kumar, U. Balakrishnan, V. Basu, Degradation process in organic thin film devices fabricated using P3HT, *Pramana* 68 (3) (2007) 489–498.
- [14] S.P. Speakman, G.G. Rozenberg, K.J. Clay, W.I. Milne, A. Ille, I.A. Gardner, E. Bresler, J.H.G. Steinke, High performance organic semiconducting thin films: ink jet printed polythiophene [rr-P3HT], *Organic Electronics* 2 (2) (2001) 65–73.
- [15] H. Klauk (Ed.), *Organic Electronics Materials, Manufacturing and Applications*, Wiley-VCH Verlag GmbH and Co., Weinheim, 2006.
- [16] S. Mijalkovic, D. Green, A. Nejim, G. Whiting, A. Rankov, E. Smith, J. Halls, C. Murphy, Modeling of organic field effect transistors for technology and circuit design, in: *Proceedings of the 26th International Conference On Microelectronics*, 2008, pp. 469–476.
- [17] S. Joshi, P. Pingel, S. Grigorian, T. Panzner, U. Pietsch, D. Neher, M. Forster, U. Scherf, Bimodal temperature behavior of structure and mobility in high molecular weight P3HT thin films, *Macromolecules* 42 (2009) 4651–4660.
- [18] S. Cho, K. Lee, Thermal annealing-induced enhancement of the field-effect mobility of regioregular poly(3-hexylthiophene) films, *Journal of Applied Physics* 100 (2006) 114503.
- [19] Y.D. Gokdel, B. Sarioglu, S. Mutlu, A.D. Yalcinkaya, Design and fabrication of two-axis micromachined steel scanners, *Journal of Micromechanics and Microengineering* 19 (7) (2009).
- [20] A.O. Sevim, S. Mutlu, Post-fabrication electric field and thermal treatment of polymer light emitting diodes and their photovoltaic properties, *Organic Electronics* 10 (1) (2009) 18–26.
- [21] A. Haldi, A. Sharma, W.J. Potscavage Jr., B. Kippelen, Equivalent circuit model for organic single-layer diodes, *Journal of Applied Physics* 104 (2008) 064503.
- [22] M. Giulianini, E.R. Waclawik, J.M. Bell, N. Motta, Current–voltage characteristics of poly(3-hexylthiophene) diodes at room temperature, *Applied Physics Letters* 94 (2009) 083302.
- [23] P.N. Murgatroyd, Theory of space-charge-limited current enhanced by Frenkel effect, *Journal of Physics D: Applied Physics* 3 (2) (1970) 151–156.
- [24] A. Takshi, A. Dimopoulos, J.D. Madden, Depletion width measurement in an organic Schottky contact using a metal-semiconductor field-effect transistor, *Applied Physics Letters* 91 (2007) 083513.
- [25] A. Takshi, J.D. Madden, Large apparent inductance in organic Schottky diodes at low frequency, *Journal of Applied Physics* 99 (2006) 084503.